No evidence for intracellular magnetite in putative vertebrate magnetoreceptors identified by magnetic screening

Nathaniel B. Edelman[a,b], Tanja Fritz[a], Simon Nimpf[a], Paul Pichler[a], Mattias Lauwers[a,1], Robert W. Hickman[a], Artemis Papadaki-Anastasopoulou[a], Lyubov Ushakova[a], Thomas Heuser[c], Guenter P. Resch[c], Martin Saunders[d], Jeremy A. Shaw[d], and David A. Keays[a,2]

[a]Institute of Molecular Pathology (IMP), Vienna Biocenter (VBC), 1030 Vienna, Austria; [b]Department of Organismic and Evolutionary Biology, Harvard University, Cambridge, MA 02138; [c]Campus Science Support Facilities, 1030 Vienna, Austria; and [d]Centre for Microscopy, Characterisation and Analysis, The University of Western Australia, Crawley, Perth, WA 6009, Australia

Edited by Sönke Johnsen, Duke University, Durham, NC, and accepted by the Editorial Board November 26, 2014 (received for review April 30, 2014)

The cellular basis of the magnetic sense remains an unsolved scientific mystery. One theory that aims to explain how animals detect the magnetic field is the magnetite hypothesis. It argues that intracellular crystals of the iron oxide magnetite (Fe_3O_4) are coupled to mechanosensitive channels that elicit neuronal activity in specialized sensory cells. Attempts to find these primary sensors have largely relied on the Prussian Blue stain that labels cells rich in ferric iron. This method has proved problematic as it has led investigators to conflate iron-rich macrophages with magnetoreceptors. An alternative approach developed by Eder et al. [Eder SH, et al. (2012) *Proc Natl Acad Sci USA* 109(30):12022–12027] is to identify candidate magnetoreceptive cells based on their magnetic moment. Here, we explore the utility of this method by undertaking a screen for magnetic cells in the pigeon. We report the identification of a small number of cells (1 in 476,000) with large magnetic moments (8–106 fAm^2) from various tissues. The development of single-cell correlative light and electron microscopy (CLEM) coupled with electron energy loss spectroscopy (EELS) and energy-filtered transmission electron microscopy (EFTEM) permitted subcellular analysis of magnetic cells. This revealed the presence of extracellular structures composed of iron, titanium, and chromium accounting for the magnetic properties of these cells. Application of single-cell CLEM to magnetic cells from the trout failed to identify any intracellular structures consistent with biogenically derived magnetite. Our work illustrates the need for new methods to test the magnetite hypothesis of magnetosensation.

magnetoreception | pigeons | magnetite

The magnetic sense is a navigational tool used by a diverse group of animal species, including newts, sea turtles, migratory birds, salmon, and pigeons (1–6). Although there is robust evidence for the existence of this sense, the molecular and cellular mechanisms that underlie it remain unresolved (7). Currently, two dominant hypotheses attempt to explain the sensory integration of magnetic information. The first, known as the radical pair hypothesis, argues that the spin state of a light-induced radical pair is influenced by the Earth's magnetic field, which, in turn, affects the biochemical properties of a signaling protein (8). This protein is hypothesized to be the blue-light sensitive molecule cryptochrome (9–11). The second concept, known as the magnetite hypothesis, argues that the magnetic iron oxide magnetite (Fe_3O_4) is coupled to a mechanosensitive ion channel. A force applied by magnetite on the channel due to magnetic influences would thereby mediate a change in the membrane potential and subsequent neuronal activation (12, 13). In birds, a light-dependent compass has been associated with the retina and a region of the avian telencephalon known as cluster N (14, 15). In contrast, the magnetite hypothesis has been associated with the ophthalmic branch of the trigeminal nerve and more recently the vestibular system (16–18).

Several groups have attempted to identify the primary sensory cells associated with an iron oxide-based magnetoreceptor (19–24). Most have used the Prussian Blue reaction which labels ferric iron. However, this method is of limited utility because it stains all iron-rich cells. This has led to the conflation of iron-rich macrophages with a conserved magnetic sense system in the upper beak of birds (22, 24). An alternative approach to identify putative magnetite-based magnetoreceptors is to exploit the innate magnetic properties of these cells. Such an approach was recently adopted by Eder et al. (25), who used an artificial magnetic field to identify magnetic cells in the trout olfactory rosette. Their system used two pairs of Helmholtz coils to produce a strong (2-mT) rotating magnetic field. Screening cells in suspension resulted in the identification of a small number of cells (1–4 in 10,000) that rotated at a frequency corresponding to the externally applied field. Measurement of their boundary frequency (the speed at which a spinning cell is no longer able to rotate in synchrony with the external field) permitted the estimation of the magnetic moment. These moments, which varied from 4 to 100 fAm^2, greatly exceeded previous estimates (26). Using reflective microscopy and the membrane marker FM1-43, they were able to identify 1- to 2-μm-sized particles close to the cell membrane, which they suggested were made up of single domain magnetite crystals. It was argued by Eder et al. that their

Significance

The list of animals that use the Earth's magnetic field as a navigation tool is long and diverse; however, the cells responsible for transducing magnetic information into a neuronal impulse have not been discovered. One hypothesis argues that these cells use an iron oxide called magnetite (Fe_3O_4). Here, we use a "magnetoscope" coupled with single-cell correlative light and electron microscopy to identify candidate magnetoreceptors in the pigeon and trout. We report that a small percentage of cells in both species appear to have large magnetic moments, but they do not contain biogenic magnetite. Our work illustrates the need for technological innovation if the true magnetoreceptors are to be found.

Author contributions: N.B.E., T.F., P.P., J.A.S., and D.A.K. designed research; N.B.E., T.F., S.N., P.P., M.L., R.W.H., A.P.-A., L.U., T.H., G.P.R., M.S., and J.A.S. performed research; N.B.E., T.F., T.H., G.P.R., M.S., J.A.S., and D.A.K. analyzed data; and N.B.E. and D.A.K. wrote the paper.

The authors declare no conflict of interest.

This article is a PNAS Direct Submission. S.J. is a guest editor invited by the Editorial Board.

Freely available online through the PNAS open access option.

[1]Deceased September 12, 2014.

[2]To whom correspondence should be addressed. Email: keays@imp.ac.at.

This article contains supporting information online at www.pnas.org/lookup/suppl/doi:10.1073/pnas.1407915112/-/DCSupplemental.

method was a highly specific and effective way to identify and characterize potential magnetite-based magnetoreceptors in a broad range of species.

Here, we explore the utility of this approach by undertaking a screen for magnetic cells in the pigeon *Columbia livia*. We report the identification of cells that exhibit a spinning behavior when exposed to a rotating magnetic field. These cells have magnetic moments that vary between 8 and 106 fAm^2 and possess distinct reflective particles associated with the cellular membrane. The development of single-cell correlative light and electron microscopy (CLEM) has revealed that these reflective particles are in fact extracellular and are almost certainly contaminants from the laboratory or the environment in which the bird lives. A subcellular analysis of spinning cells from the rainbow trout, *Oncorhynchus mykiss*, has likewise revealed the absence of intracellular magnetite, and instead the presence of extracellular contaminants.

Results

A Screen for Magnetic Cells in the Pigeon. To identify cells in the pigeon with magnetic properties, we built a "magnetoscope" by modifying an inverted light microscope (Zeiss Axiovert 135) replacing the metal stage with a plastic one and installing a rotating neodymium finger magnet below the condenser that produces a field of either 2 or 10 mT (magnetoscope A; Fig. S1*A*). We confirmed that this apparatus has the ability to elicit spinning behavior in cells that possess magnetite by analyzing the magnetotactic bacteria *Magnetospirillum magnetotacticum* (DSM 3856). For our pigeon experiments, we dissected out our tissues of interest (n = 10 birds), lightly dissociated them, and then fixed them with paraformaldehyde before screening isolated cells on the magnetoscope using a 10-mT field. We chose to screen the lagena, the basilar papilla, the olfactory epithelium, the ventral surface of the upper beak, and the retina as they have been implicated in magnetosensation (15, 16, 27, 28). We also included the dorsal surface of the upper beak, skin from the abdomen, the respiratory concha, and the spleen to establish whether iron-rich cells, such as macrophages, also exhibit spinning behavior. To limit contamination from the laboratory environment, all coverslips were acid washed, all dissections were performed with titanium or ceramic-coated tools, and we placed plastic film over laboratory surfaces (Saran Wrap). A cell was classified as a spinning cell if the following criteria were met: (*i*) the cell spun in synchrony with the magnet; (*ii*) the cell was isolated and not part of an undigested group of cells; and (*iii*) the cell was positive for the nuclear stain Hoechst. We excluded cells if they were associated with large particulates that were clearly extracellular. We screened in excess of 6.6 million dissociated cells and identified 14 cells that met the aforementioned criteria (1 in 476,000) (Fig. 1 *A–C* and Movies S1 and S2). These were found in the lagena (4 cells; 0.0162% of cells), the basilar papilla (7 cells; 0.003% of cells), the dorsal upper beak skin (2 cells; 0.0015% of cells), and the olfactory epithelium (1 cell; 0.0006% of cells) (Fig. 1*D*). Combined, the basilar papilla and the lagena had 11 of the 14 cells (79%). Meanwhile, the dorsal upper beak contained 2 out of 14 (14%), and the olfactory epithelium yielded 1 out of 14 (7%) (Fig. 1*E*). We identified no spinning cells in the spleen indicating that the iron-rich macrophages (which are abundant in this tissue) do not spin (29). To ascertain whether the observed spinning cells comprised a single morphological class, we analyzed their appearance using both transmitted light and fluorescent imaging staining with the membrane marker FM1-43 (Fig. 2 *A–L* and Fig. S2 *A–L*). Although the cells from different tissues bore no obvious similarities, one class was apparent in the cells originating from the cochlear duct. The cells belonging to this category (6 of the 11 found in this tissue) had a rounded, rough region with a distinctive "broccoli"-shape morphology (Fig. 2 *A* and *E*, and Fig. S2*A*).

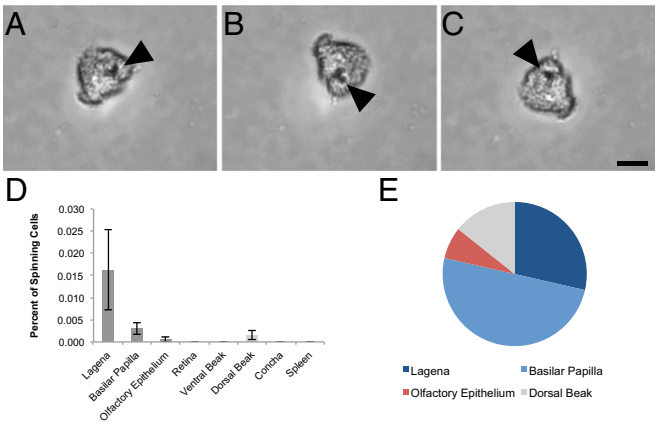

Fig. 1. Results of magnetic cell screening. Tissue dissociates were exposed to a rotating magnetic field, and magnetic cells were identified by their spinning behavior. (*A–C*) Sequential images of a rotating cell from the inner ear lagena. An opaque inclusion is indicated with the arrow. (Scale bar: 10 μm.) (*D*) Percentage of cells with magnetic properties by tissue (mean ± SEM). We observed the highest percentage of spinning cells in the lagena and basilar papilla. (*E*) Proportion of total magnetic cells in each tissue (n = 10 birds, n = 14 spinning cells, $n \geq$ 6.6 million cells screened).

The Magnetic Moment of Spinning Cells in the Pigeon. We focused on those spinning cells in the cochlear duct (i.e., the basilar papilla and lagena) and the olfactory epithelium as they contain a wealth of sensory cells. To determine whether these cells could act as transmitters of earth-strength magnetic field changes, we measured their magnetic moment. To do so, we constructed a second magnetoscope (magnetoscope B) whereby two pairs of Helmholtz coils were driven by bipolar relays, allowing the generation of uniform rotating fields with a gradient of intensities up to 2 mT (Fig. S1*B*). We screened dissociated cells from the olfactory epithelium and cochlear duct with magnetoscope B (n = 6 birds), measuring their boundary frequency. Moments varied from 8 to 106 fAm^2, with the majority (6 of 8) between 8 and 40 fAm^2 (n = 8 cells; Fig. S3 and Table S1). These results are analogous to those obtained by Eder et al., who observed cells with moments spanning 4–100 fAm^2, with the majority (11 of 13) between 10 and 50 fAm^2 (25). To establish whether the cells possess remanent magnetism or alternatively superparamagnetism, we determined the moment at a variety of different magnetic intensities (0.5, 1, 1.25, 1.5, 1.75, and 2 mT). If a cell has superparamagnetic properties, an increase in external field strength would result in an increase in magnetic moment (30). With the exception of one cell, we observed no such dependence (Fig. S3 and Table S1), indicating the presence of remanence-bearing particles.

The Subcellular Architecture of Spinning Cells in the Pigeon. In the pervasive model of magnetite-based magnetoreception, a chain of magnetite particles is coupled to a membrane-bound mechanosensitive ion channel (13). To determine whether spinning cells have a subcellular architecture consistent with this model, we developed single-cell CLEM, coupled with transmitted, fluorescent, and reflective light microscopy. This method required the screening of dissociated cells for spinning behavior on magnetoscope A, which is equipped with a micromanipulator (Fig. S1*A*). Hoechst-positive spinning cells were visualized with reflective light microscopy, permitting the identification of structures that might be crystalline and could potentially be responsible for the magnetic properties of the cell. These cells were then picked and placed on circular Aclar discs embossed with a patterned grid and coated with poly-L-lysine. Following fixation with osmium tetroxide, the Aclar disk was carefully dehydrated and embedded in

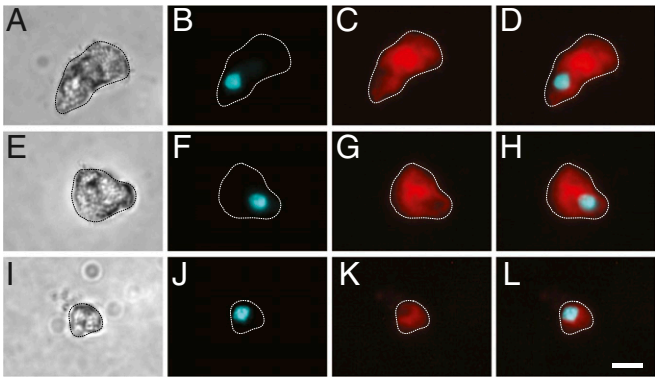

Fig. 2. Morphology of spinning cells. Dissociated cells were stained with the membrane marker FM1-43 and the nuclear Hoechst stain to confirm the cellular nature of spinning objects. (*A*, *E*, and *I*) Representative transmitted light images of magnetic cells from the lagena (*A* and *E*) and the olfactory epithelium (*I*). (*B*, *F*, and *J*) Fluorescent images of cells stained with Hoechst (shown in cyan). (*C*, *G*, and *K*) Fluorescent images of cells stained with FM1-43 (shown in red). (*D*, *H*, and *L*) Shows merged images. The periphery of cells (dashed lines) was defined by the FM1-43 staining. (Scale bar: in *L*, 10 μm.)

Epon. When the Aclar disk was removed, an embossed grid pattern remained on the block, permitting the precise location of individual cells. This cell was then subject to serial sectioning and imaged (Fig. S4 *A*–*F*).

We validated this approach with a sample of *Magnetospirillum magnetotacticum*, confirming that the integrity of magnetite crystals is preserved by the method (Fig. S4 *G* and *H*). Next, we screened additional cell dissociates resulting in the identification and subsequent imaging of six spinning cells from the olfactory epithelium and seven from the cochlear duct (Fig. 3 *A*–*L*). Each cell had at least one reflective structure associated with the cell membrane; however, it was not possible to determine whether the particles were intracellular or extracellular using light microscopy (Fig. 3 *A*, *D*, *G*, and *J*). Analysis of the electron micrographs for each of these cells revealed that, in all cases, there was a conspicuous electron-dense structure (corresponding to the position of the reflective particle) that was external to the cell membrane (Fig. 3 *B* and *C*, *E* and *F*, *H* and *I*, and *K* and *L*). These electron-dense structures were not uniform in size or shape and in some instances were an agglomeration of electron-dense particles (Fig. 3*E*).

To determine the elemental makeup of these structures, we performed electron energy loss spectroscopy (EELS) and energy-filtered TEM (EFTEM) (Fig. 4 *A*–*D*). We analyzed the composition of electron-dense structures attached to the cell ($n = 11$ cells). This revealed the presence of iron and oxygen ($n = 10$ cells), as well as titanium ($n = 6$ cells), chromium (2 cells), aluminum ($n = 2$ cells), cobalt ($n = 1$ cell), and silicon ($n = 2$ cells) (Table S2). These data strongly suggest that the extracellular particles are not of biological origin. In two instances (P-F, P-G), elemental analysis coupled with selected area electron diffraction (SAED) revealed the presence of extracellular structures consistent with magnetite crystals (Fig. S5 *A*–*D* and Table S3). These crystals were almost identical in size and shape to commercial magnetite particles (Nanostructured and Amorphous Materials; 265OTR) used in the laboratory as a positive control for Prussian Blue staining (Fig. S5 *E* and *F*). An extensive search in structurally intact cochlear ducts ($n = 3$) by serial sectioning TEM failed to find similar crystals, leading us to the conclusion that they are contaminants from the laboratory environment. In two further instances, the extracellular structures contained only iron and oxygen (P-H, P-J) but when analyzed with SAED did not produce diffraction patterns that permitted determination of their mineral phase. These structures were irregular in size, amorphous, and extracellular, again suggesting they are contaminants (Fig. S6).

Finally, we considered the possibility that groups of cells, and/or those structures that were negative for nuclear markers might be magnetoreceptors. To investigate this, we performed CLEM coupled with EELS on groups of cells that spun ($n = 6$) and FM1-43–positive cellular fragments that were Hoechst negative ($n = 6$). This once again revealed the presence of electron-dense structures that were not consistent with biogenic magnetite (Fig. S7 and Tables S4 and S5).

The Subcellular Architecture of Magnetic Cells in the Trout. Next, we asked whether magnetic cells in the trout have a subcellular architecture consistent with a role in magnetosensation, or alternatively if their spinning behavior might also be explained by contamination. To investigate this, we lightly dissociated and fixed cells from the olfactory rosette of juvenile trout (Austrian cohort) (25). We then screened these cells using a 2-mT field rotating at 0.33 Hz [the same parameters used by Eder et al. (25)]. We screened 3.6 million cells ($n = 10$ trout), leading to the identification of 7 spinning cells (1 in 520,000), each of which was positive for the nuclear marker Hoechst (Movies S3 and S4, and Fig. 5 *A*–*C*). The morphology of these cells mirrored those previously reported, each with a notable opaque structure associated with the membrane (25). Assessment of their magnetic moment revealed that they vary between 2 and 152 fAm^2, and have a profile consistent with the presence of remanence-bearing particles (Fig. 5*D* and Table S6). The screening of 2.2 million cells from a second population of trout (Munich cohort) ($n = 18$ trout) yielded similar results, with 1 in 309,000 cells exhibiting spinning behavior.

To investigate the subcellular architecture of magnetic cells, we screened dissociated cells with magnetoscope A (using both

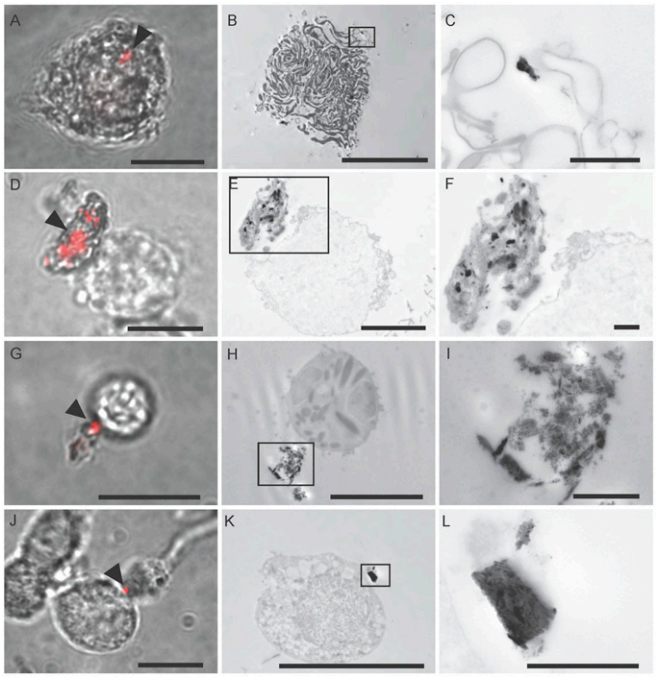

Fig. 3. Single-cell CLEM results. Single-cell CLEM was used to identify particles associated with spinning cells from the cochlear duct (*A*–*F*) and the olfactory epithelium (*G*–*L*). (*A*, *D*, *G*, and *J*) Merged reflective and transmitted light images of spinning cells at 100× magnification. The reflective particles are shown in red and are indicated with arrows. (Scale bars: 10 μm.) (*B*, *E*, *H*, and *K*) Single-cell CLEM was performed on those cells. In each case, an electron-dense structure was identified in the same location as the reflective particle and external to the cell membrane. (Scale bars: in *B*, *H*, and *K*, 10 μm; in *E*, 5 μm.) (*C*, *F*, *I*, and *L*) High-magnification images of the boxed areas in *B*, *E*, *H*, and *K*. (Scale bars: 1 μm.)

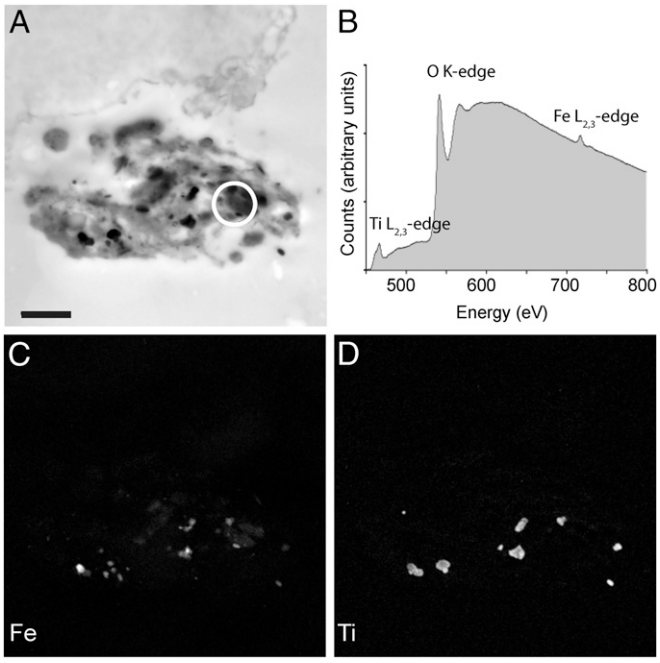

Fig. 4. Elemental analysis of spinning cells. (*A*) High-magnification TEM micrograph of the electron-dense extracellular structure associated with the spinning cell shown in Fig. 3 *E* and *F*. The structure shown in Fig. 4*A* is a mirror image of that shown in Fig. 3 *E* and *F*, as the image was captured on a different microscope. (Scale bar: 1 μm.) (*B*) Background-corrected electron energy loss spectra (EELS) obtained from the circled region in *A*. Titanium, oxygen, and iron were detected. Using energy-filtered transmission electron microscopy (EFTEM), element maps were generated for iron (*C*) and titanium (*D*). These elements are found throughout the extracellular aggregate, strongly suggesting that they are contaminants.

2- and 10-mT fields), and performed single-cell CLEM ($n = 6$ cells) combined with reflective light microscopy and EELS ($n = 6$ cells) (Austrian cohort) (Fig. 5 *E–L*). We failed to identify any structures consistent with intracellular magnetite; instead, we again observed extracellular electron-dense particles that consisted of iron and oxygen ($n = 6$), and in some instances also included chromium ($n = 3$), titanium ($n = 2$), or silicon ($n = 1$) (Fig. 5 *H–L*, Fig. S6, and Table S2).

Discussion

The aim of this study was to identify putative magnetite-based magnetoreceptors in the pigeon *Columbia livia* and to investigate their ultrastructure. Using two custom-built magnetoscopes, we identified a small number of cells (1 in 476,000) with large magnetic moments (8–106 fAm^2) that were most often found in the lagena and basilar papilla. The development of single-cell CLEM permitted the subcellular analysis of these cells. Coupled with EELS and EFTEM, it revealed the presence of electron-dense extracellular objects, which are made up of a variety of elements including iron, titanium, silicon, and chromium. Similar structures and reflective particles were also found in magnetic cells isolated from the trout, which again were rare (1 in 520,000) and possessed large moments (2 and 152 fAm^2).

The fundamental issue at hand is the following: do magnetic cells spin because of an intracellular biogenic magnetite-based magnetoreceptor, or do they spin because of an attached iron-based contaminant? The data we have generated strongly supports the latter proposition. All electron-dense structures visualized by CLEM in both pigeons and trout were extracellular, and the majority contained titanium or chromium, which cannot be generated biogenically. The magnetic moments we have observed, and those reported by Eder et al., support the contention that magnetic cells spin because of contamination. First, there is a large variation in the moments from one cell to the next. One explanation might be that both trout and pigeons have a suite of genetically encoded magnetoreceptors with different and specific magnetic moments. However, the simpler and more reasonable explanation is that different moments are a consequence of the different sizes and compositions of contaminating particles. Second, the moments described by both Eder and ourselves are large. Assuming that pigeons and trout use single-domain magnetite crystals of ~40 nm in size (that have a volume of 5×10^4 nm^3), about 1,600 individual crystals would be required to generate a moment of 40 fAm^2. Such large numbers of intracellular crystals would be readily identified by TEM, but despite an extensive search throughout the cochlear duct and in isolated spinning cells none have been found.

What is the source of contamination? In performing our experiments, we were conscious of the risk of external contamination from the laboratory environment; however, it is evident from this study that a certain amount of iron contamination is unavoidable. This is a particular risk for those laboratories working on magnetite-based magnetoreception where magnetotactic bacteria and commercial nanoparticles are often used as positive controls. The latter appears to be the source of contamination in at least two cells we have analyzed. The presence of silicon in a number of spectra we have obtained suggests that either the ceramic-coated tools we used, or iron particles embedded in glassware might be the source. Alternatively, it is entirely possible that small iron contaminants within commercially supplied reagents (e.g., NaCl, KCl, $CaCl_2$, $MgCl_2$) that were subject to saturation magnetization were the source of contamination.

Why did we find so few spinning cells? We found that only 1 in 476,000 cells in the pigeon spin, 1 in 520,000 cells from our Austrian trout cohort spin, and 1 in 309,000 cells from the Munich trout spin. This is a sharp contrast to that reported by Eder et al. (25), who reported that between 1 and 4 in 10,000 cells spin from the trout olfactory rosette. We can exclude the possibility that this difference is due to the trout themselves as the Munich trout we used are from the same source as those of Eder et al. Might the difference in spinning cell number be due to the protocols used? We followed the methods of Eder et al. closely. Like them, we dissociated the cells in Ringer's with 0.25 mg/mL papain activated with 1.25 mg/mL L-cystein, followed by tituration. Like them, we screened cells on silanated slides using a 2-mT field rotating at 0.33 Hz. However, we digested our cells in papain for 7 min in preference to 10 min. We chose a shorter digestion time because we found it improved the integrity of cells. Similarly, we chose to fix the cells following dissociation because it preserved their morphology and was essential for the subsequent subcellular and elemental analysis using TEM. We think these methodological differences are very unlikely to account for the discrepancy in spinning cell number. If anything, we would expect that fixation would strengthen the association of biogenic magnetite to any cellular structures and increase the percentage of spinning cells. One explanation for this difference in spinning cell numbers between the two groups could be the stricter criteria we adopted in defining a magnetic cell; specifically, we required the presence of a Hoechst-positive nucleus. We have also very carefully quantitated the total number of cells per a sample to accurately reflect the number of cells that we screened and the number that spun. Alternatively, the difference in the prevalence of spinning cells might reflect differences in the levels of contaminating magnetic particles.

Walker and colleagues (26) have previously used reflective confocal microscopy coupled with magnetic force microscopy, arguing there is a population of multilobed cells in the olfactory rosette of the trout that contain 1-μm chains of magnetic crystals with a magnetic moment of 0.5 fAm^2. Our results do not exclude

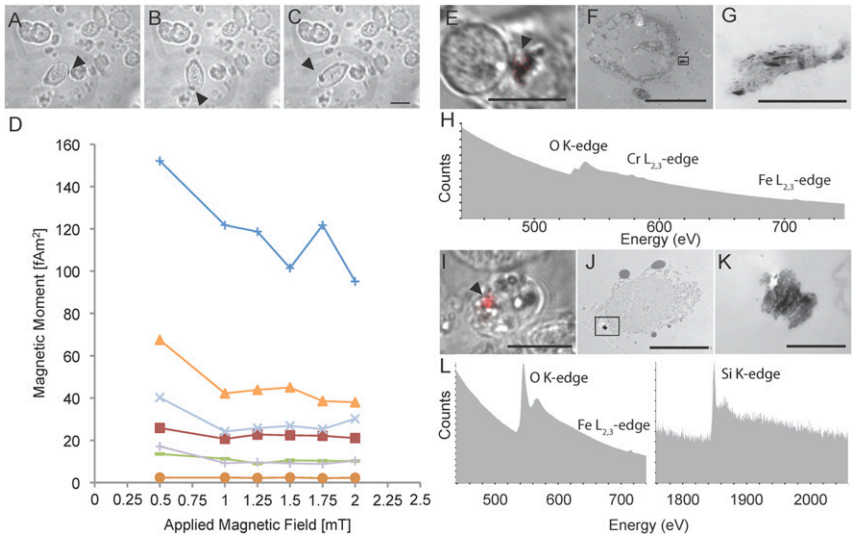

Fig. 5. Analysis of spinning cells in the trout. (*A–C*) Sequential images of a rotating cell from the olfactory rosette. An opaque inclusion is indicated with the arrow. (*D*) Magnetic moment of spinning cells isolated from the olfactory rosette of trout. The moments vary between 2 and 152 fAm^2 ($n = 7$ cells). The applied magnetic field is shown on the *x* axis and the calculated moment on the *y* axis. (*E–G* and *I–K*) CLEM of two spinning cells from the trout olfactory rosette. (*E* and *I*) Merged transmitted light and reflected light images of two spinning cells. The reflective particle is shown in red and is indicated with an arrow. (*F* and *J*) An overview TEM image of these cells. (*G* and *K*) High-magnification images of the electron-dense structures boxed in *F* and *J*. (*H* and *L*) Raw electron energy loss spectra (EELS) obtained from structures attached to the cells shown in *E* and *I*. These sections were neighboring to those shown in *G* and *K*. In *H*, we detected iron and chromium, and in *L*, silicon and iron, but no chromium or titanium. (Scale bars: in *C*, *E*, *I*, and *F*, 10 μm; in *G*, 1 μm; in *J*, 5 μm; in *K*, 500 nm.)

the possibility that such a magnetite-based magnetoreceptor exists, as only cells with a moment above 2 fAm^2 exhibited spinning behavior in our screen.

The majority of spinning cells we identified in the pigeon originated from the inner ear. What might be the explanation for this? Of the 11 spinning cells we identified in the lagena and basilar papilla in our initial screen, 6 had a very distinct broccoli-shape morphology. TEM analysis revealed that these cells have a subcellular architecture consistent with dark cells, which are found in the extensively vascularized tegmentum vasculosum (31). Dark cells, which are believed to play a role in endolymph generation, have an electron-dense organelle-rich cytoplasm, which is expanded basally by extensive membrane infoldings (Fig. 3 *A–C*) (32). It is possible that contaminants are more likely to attach to this expansive membranous area, resulting in an enrichment of spinning cells in inner ear tissues.

There is undeniably strong evidence supporting magnetosensation in birds, but still the primary sensory cells have not been identified (2). So where are they? In addition, do they necessarily have to be magnetite based? Regions innervated by the ophthalmic branch of the trigeminal nerve, along with the vestibular system remain the most promising anatomical locations for the magnetosensors (16, 33). Although a trigeminal-based magnetoreceptor need not necessarily be iron dependent, the vestibular recordings performed by Dickman and colleague (17) in the absence of light provide the best evidence for a magnetite-based magnetoreceptor in the pigeon inner ear. We have recently discovered that some hair cells in the pigeon contain an iron-rich organelle in the cuticular plate. However, current evidence suggests that this structure is composed of ferrihydrite and therefore lacks the magnetic properties necessary to act as a torque-based magnetoreceptor (27). It nonetheless remains possible that such a magnetite-based receptor does exist, possessing sufficient magnetic moment to open a mechanosensitive channel but insufficient moment to spin a cell. How might such a receptor be found? Our experience suggests that isolating cells with spinning behavior is not a productive course, as it is extremely laborious and has failed to reliably identify cells associated with the magnetic sense. One way forward might be to use advanced electron microscopy techniques, such as focused ion beam or serial block face-scanning electron microscopy coupled with an elemental detector (34). The development of such a technique would allow cubic millimeters of tissue to be screened at a subcellular resolution for magnetite crystals. Alternatively, investment in high-throughput optical magnetic imaging tools based on nitrogen-vacancy quantum spin states might be productive (35). Our work demonstrates the necessity for this, or other such innovation, in the ongoing search for the vertebrate magnetoreceptor.

Materials and Methods

Pigeon Tissue Dissection and Dissociation. We used adult racing pigeons aged approximately 1 y from our Vienna cohort. Experiments were performed in accordance with the relevant guidelines and regulations (Magistrat 60, MA60-001603/2010/002). These animals were provided with a mixed seed source of food (Hesa Saaten; catalog nos. 603094, 603096). Animals were killed, and the tissues of interest were dissected in ice-cold Ringer's solution (145 mM NaCl, 5 mM KCl, 1 mM $CaCl_2$, 1 mM $MgCl_2$, 5 mM glucose, 20 mM Hepes, pH 7.4) with ceramic-coated or titanium dissection tools. The tissues were then cut into small pieces (~2 mm^3) to aid digestion and dissociated. In the case of the lagena and basilar papilla, the tissue was dissociated in its entirely. In the case of the respiratory concha, the retina, the olfactory epithelium, and the dorsal and ventral beak skins we sampled along the length of the beak, throughout the retina and olfactory epithelium, and both the lateral and medial regions of the respiratory concha. Tissues were dissociated in 0.05% trypsin-EDTA (GIBCO; 15400-054) in PBS at 37 °C for 5–7 min (pH 7.4). Immediately after the dissociation, a trypsin inhibitor (Sigma-Aldrich; T9128) was added at a 1:1 ratio. Cell suspensions were then passed through a 70-μm nylon filter mesh (BD Falcon; 352350), and an equal volume of 4% (wt/vol) PFA was added (pH 7.4). Cells used for electron microscopy were fixed with equal volumes of 8% PFA/5% (wt/vol) glutaraldehyde (pH 7.4). Cells were further stained with the membrane marker FM1-43FX (Invitrogen; F-35355; 5 μM) and the nuclear marker Hoechst 33258 (Invitrogen; H3569; 16 μM).

Pigeon Cell Screening. All dissociated tissue samples were blinded with random numerical sequences, and two 75-μL aliquots were screened. In each instance, samples were screened in a chamber (9.5 mm × 9.55 mm × 1 mm; Sigma; GBL103330), sandwiched between two acid-washed coverslips that

had been silanated (Sigmacote; Sigma SL2), rendering them hydrophobic. The initial pigeon screen was performed on magnetoscope A (Fig. S1*A*). The magnet rotated at a frequency of 0.25 Hz and rendered a field of ∼10 mT on the sample. When a spinning object was observed, it was categorized as cellular or noncellular based on the membrane marker FM1-43FX (Invitrogen; F-35355) and the nuclear marker Hoechst 33258 (Invitrogen; H3569). The total number of Hoechst-positive cells in five different areas (530 × 395 μm) of the sample was counted at 20× magnification. The average count was multiplied by a scale factor of 432 to extrapolate the total number of cells in the well. To obtain the percentage of spinning cells, the number of spinning cells was divided by this value. To visualize reflective particles, filter sets were removed from the incident light path and reflective light captured. Pictures and movies were taken with a SPOT Idea 1.3 megapixel camera (Visitron Systems). Image processing was performed with ImageJ.

Single-Cell CLEM and Elemental Analysis. A detailed description of single-cell CLEM can be found in *SI Materials and Methods*. Briefly, cells were picked and fixed onto carbon-embossed Aclar discs. Following dehydration, they were embedded in epoxy resin, trimmed, and sectioned. EELS and EFTEM were conducted as described previously (24).

Magnetic Moment Measurement. The magnetic moment was determined using magnetoscope B (Fig. S1*B*), drawing on the methods applied by Eder et al. (25). Following the identification of a spinning cell, the frequency of rotation was steadily increased until the cell could no longer smoothly rotate with the field. This boundary frequency was calculated using the following field strengths (0.5, 1, 1.25, 1.5, 1.75, and 2 mT) and used to determine the magnetic moment of the cell. (See *SI Materials and Methods* and Tables S1 and S6.)

Trout Tissue Dissection and Dissociation. Trout ∼20 cm in length were sourced from Forellenhof Piringer, Gloggnitz, Austria, and were kept on a diet of Aquastart (Garant-Tiernahrung) (Austrian cohort). Trout ∼10 cm in length were sourced from Mauka Fish Farm, Massenhausen, Germany, and fed Pro Aquabrut (Skretting) (Munich cohort). Fish were killed, and the olfactory rosette was dissected in ice-cold Ringer's solution using ceramic-coated and titanium tools. Papain (0.25 mg/mL; Sigma-Aldrich; P3375) was activated by L-cystein (1.25 mg/mL; Sigma-Aldrich; C7352) in calcium-free Ringer's solution for 10 min. The rosettes were then dissociated in this solution for 7 min. Leupeptin hemisulfate salt (0.05%; Sigma-Aldrich; L2884) was then added to inhibit the papain and the cells triturated with a pipette for a further 7 min. Cells were then fixed with equal volumes of 8% (wt/vol) PFA/5% glutaraldehyde and stained with Hoechst (Invitrogen; H3569; 16 μM). The total number of cells screened and the percentage that spun was calculated as described for the pigeon screen.

ACKNOWLEDGMENTS. We are indebted to Prof. Michael Winklhofer and Stefan Eder for their assistance in building our magnetoscopes and for hosting Nathaniel Edelman in their laboratory. We thank the Bio-optics, Histology, Electron Microscopy, and Graphics Departments at the Institute of Molecular Pathology and the Campus Science Support Facilities. Gratitude is also owed to the Centre for Microscopy, Characterization and Analysis and the Australian Microscopy and Microanalysis Research Facility at the University of Western Australia, a facility funded by the University, State and Commonwealth Governments. D.A.K. is a European Molecular Biology Organization Young Investigator and is supported by the European Research Council (336724) and Fonds zur Förderung der Wissenschaftlichen Forschung (Y726). We express our sincere thanks to Boehringer Ingelheim, which funds basic biological research at the Institute of Molecular Pathology.

1. Lohmann KJ (1991) Magnetic orientation by hatchling loggerhead sea turtles (*Caretta caretta*). *J Exp Biol* 155:37–49.
2. Mouritsen H, Hore PJ (2012) The magnetic retina: Light-dependent and trigeminal magnetoreception in migratory birds. *Curr Opin Neurobiol* 22(2):343–352.
3. Walcott C (1991) Magnetic maps in pigeons. *EXS* 60:38–51.
4. Putman NF, et al. (2014) An inherited magnetic map guides ocean navigation in juvenile Pacific salmon. *Curr Biol* 24(4):446–450.
5. Wiltschko W, Wiltschko R (1972) Magnetic compass of European robins. *Science* 176(4030):62–64.
6. Phillips J, Borland S (1994) Use of a specialized magnetoreception system for homing by the eastern red-spotted newt *Notophthalmus viridescens*. *J Exp Biol* 188(1):275–291.
7. Lohmann KJ, Johnsen S (2000) The neurobiology of magnetoreception in vertebrate animals. *Trends Neurosci* 23(4):153–159.
8. Ritz T, Adem S, Schulten K (2000) A model for photoreceptor-based magnetoreception in birds. *Biophys J* 78(2):707–718.
9. Gegear RJ, Casselman A, Waddell S, Reppert SM (2008) Cryptochrome mediates light-dependent magnetosensitivity in *Drosophila*. *Nature* 454(7207):1014–1018.
10. Gegear RJ, Foley LE, Casselman A, Reppert SM (2010) Animal cryptochromes mediate magnetoreception by an unconventional photochemical mechanism. *Nature* 463(7282):804–807.
11. Nießner C, et al. (2013) Magnetoreception: Activated cryptochrome 1a concurs with magnetic orientation in birds. *J R Soc Interface* 10(88):20130638.
12. Cadiou H, McNaughton PA (2010) Avian magnetite-based magnetoreception: A physiologist's perspective. *J R Soc Interface* 7(Suppl 2):S193–S205.
13. Kirschvink JL, Walker MM, Diebel CE (2001) Magnetite-based magnetoreception. *Curr Opin Neurobiol* 11(4):462–467.
14. Mouritsen H, et al. (2004) Cryptochromes and neuronal-activity markers colocalize in the retina of migratory birds during magnetic orientation. *Proc Natl Acad Sci USA* 101(39):14294–14299.
15. Zapka M, et al. (2009) Visual but not trigeminal mediation of magnetic compass information in a migratory bird. *Nature* 461(7268):1274–1277.
16. Wu LQ, Dickman JD (2011) Magnetoreception in an avian brain in part mediated by inner ear lagena. *Curr Biol* 21(5):418–423.
17. Wu LQ, Dickman JD (2012) Neural correlates of a magnetic sense. *Science* 336(6084):1054–1057.
18. Mora CV, Davison M, Wild JM, Walker MM (2004) Magnetoreception and its trigeminal mediation in the homing pigeon. *Nature* 432(7016):508–511.
19. Presti D, Pettigrew JD (1980) Ferromagnetic coupling to muscle receptors as a basis for geomagnetic field sensitivity in animals. *Nature* 285(5760):99–101.
20. Beason RC, Nichols JE (1984) Magnetic orientation and magnetically sensitive material in a transequatorial migratory bird. *Nature* 309(10):151–153.
21. Falkenberg G, et al. (2010) Avian magnetoreception: Elaborate iron mineral containing dendrites in the upper beak seem to be a common feature of birds. *PLoS One* 5(2):e9231.
22. Fleissner G, et al. (2003) Ultrastructural analysis of a putative magnetoreceptor in the beak of homing pigeons. *J Comp Neurol* 458(4):350–360.
23. Williams MN, Wild JM (2001) Trigeminally innervated iron-containing structures in the beak of homing pigeons, and other birds. *Brain Res* 889(1-2):243–246.
24. Treiber CD, et al. (2012) Clusters of iron-rich cells in the upper beak of pigeons are macrophages not magnetosensitive neurons. *Nature* 484(7394):367–370.
25. Eder SH, et al. (2012) Magnetic characterization of isolated candidate vertebrate magnetoreceptor cells. *Proc Natl Acad Sci USA* 109(30):12022–12027.
26. Diebel CE, Proksch R, Green CR, Neilson P, Walker MM (2000) Magnetite defines a vertebrate magnetoreceptor. *Nature* 406(6793):299–302.
27. Lauwers M, et al. (2013) An iron-rich organelle in the cuticular plate of avian hair cells. *Curr Biol* 23(10):924–929.
28. Walker MM, et al. (1997) Structure and function of the vertebrate magnetic sense. *Nature* 390(6658):371–376.
29. Meguro R, et al. (2005) The presence of ferric and ferrous iron in the nonheme iron store of resident macrophages in different tissues and organs: Histochemical demonstrations by the perfusion-Perls and -Turnbull methods in the rat. *Arch Histol Cytol* 68(3):171–183.
30. Cullity BD, Graham CD (2009) *Introduction to Magnetic Materials* (Wiley, Piscataway, NJ).
31. Hara J, et al. (2002) Avian dark cells. *Eur Arch Otorhinolaryngol* 259(3):121–141.
32. Hossler FE, Olson KR, Musil G, McKamey MI (2002) Ultrastructure and blood supply of the tegmentum vasculosum in the cochlea of the duckling. *Hear Res* 164(1-2):155–165.
33. Heyers D, Zapka M, Hoffmeister M, Wild JM, Mouritsen H (2010) Magnetic field changes activate the trigeminal brainstem complex in a migratory bird. *Proc Natl Acad Sci USA* 107(20):9394–9399.
34. Hughes L, Hawes C, Monteith S, Vaughan S (2014) Serial block face scanning electron microscopy—the future of cell ultrastructure imaging. *Protoplasma* 251(2):395–401.
35. Le Sage D, et al. (2013) Optical magnetic imaging of living cells. *Nature* 496(7446):486–489.